Heliyon 11 (2025) e41321

Contents lists available at ScienceDirect

Heliyon

journal homepage: www.cell.com/heliyon

Research article

Novel coumarin-based acetohydrazide-1,2,3-triazole derivatives as urease enzyme inhibitors: Synthesis, *in vitro* evaluation, and molecular dynamics simulation studies

Hassan Sepehrmansourie [a], Mohammad Azimi [b], Ahmad Ebadi [b,c], Gholamabbas Chehardoli [b,c], Mohammad Ali Zolfigol [d], Massoud Amanlou [e], Mohammad Nazari Montazer [e], Mohammad Mahdavi [f], Zahra Najafi [b,c,*]

[a] *Faculty of Converging Science and Technologies, University of Qom, Qom, Iran*
[b] *Department of Medicinal Chemistry, School of Pharmacy, Hamadan University of Medical Sciences, Hamadan, Iran*
[c] *Medicinal Plants and Natural Products Research Center, Institute of Cancer, Avicenna Health Research Institute, Hamadan University of Medical Sciences, Hamadan, Iran*
[d] *Department of Organic Chemistry, Faculty of Chemistry and Petroleum Sciences, Bu-Ali Sina University, Hamedan, Iran*
[e] *Department of Medicinal Chemistry, Faculty of Pharmacy, Tehran University of Medical Sciences, Tehran, Iran*
[f] *Endocrinology and Metabolism Research Center, Endocrinology and Metabolism Clinical Sciences Institute, Tehran University of Medical Sciences, Tehran, Iran*

ARTICLE INFO

Keywords:
Coumarin
Acetohydrazide
1,2,3-Triazole
Urease inhibition
Molecular docking
Molecular dynamics simulations

ABSTRACT

Urease enzyme inhibition is a well-established and promising strategy for preventing the harmful effects of ureolytic bacterial infections, particularly those caused by *H. pylori*. However, acetohydroxamic acid, the only approved urease inhibitor, has limited use due to significant side effects, including teratogenicity and psycho-neurological symptoms. To discover new inhibitors, novel coumarin-based acetohydrazide-1,2,3-triazole derivatives were synthesized and evaluated for their urease inhibitory activity. All tested compounds displayed remarkable anti-urease activity (IC_{50} = 1.62–16.91 μM) compared to thiourea as reference standard (IC_{50} = 23.11 ± 1.02 μM). The most potent derivative,(E)-N'-(4-((1-Benzyl-1H-1,2,3-triazol-4-yl)methoxy)benzylidene)-2-((4,7-dimethyl-2-oxo-2*H*-chromen-5-yl)oxy)acetohydrazide (**13a**), acted as an uncompetitive inhibitor with a Ki of 1.99 μM. The stable enzyme-inhibitor complex in molecular dynamics simulations (MD) indicated critical interactions between the ligand and the Cys592 and His593 residues, which stabilize the flap motif of the enzyme. Molecular dynamics simulations suggested that compound **13a** tends to remain near the SER579-HIS593 α-helix rather than the nickel ions, stabilizing it in an open state. Thus, the MD studies confirmed the proposed mechanism of uncompetitive inhibition. Overall, these findings highlight the potential of coumarin-based acetohydrazide-1,2,3-triazole hybrids as potent and novel inhibitors for developing new therapeutics against urease-related diseases.

* Corresponding author. Department of Medicinal Chemistry, School of Pharmacy, Hamadan University of Medical Sciences, Hamadan, Iran. najafi.zch@gmail.com

E-mail addresses: z.najafi@umsha.ac.ir, najafi.zch@gmail.com (Z. Najafi).

https://doi.org/10.1016/j.heliyon.2024.e41321
Received 29 August 2024; Received in revised form 8 December 2024; Accepted 17 December 2024
Available online 18 December 2024

1. Introduction

Urease is a nickel-containing metalloenzyme that catalyzes the hydrolysis of urea into ammonium and carbon dioxide [1–3]. The activity of this enzyme in microorganisms, particularly *Helicobacter pylori*, is a crucial factor in the persistence and virulence of certain pathogenic infections [4,5]. By breaking down urea, urease helps maintain an alkaline environment favorable for the survival [6,7] and proliferation of specific pathogens within the host [8–10]. Complications arising from the presence of *H. pylori* urease can lead to various health issues, such as peptic ulcers, gastric cancer, duodenal ulcers, and in some cases, stomach cancer [11]. Unfortunately, the bacterium has shown increasing antimicrobial resistance over the past decade [12]. Identifying novel antimicrobial compounds to combat this pathogen, particularly those that inhibit urease, is vital since this enzyme plays an essential role in the bacteria's survival [13]. Bacterial and plant ureases exhibit high sequence similarity and are homologous, confirming that they possess similar three-dimensional structures and a conserved catalytic mechanism [14,15]. heterocycles has been extensively utilized in the development of urease inhibitor compounds [3,16–19]. Coumarin is one of the most important heterocycles utilized in the design of new compounds due to its diverse biological and medicinal activities [20,21]. As shown in Fig. 1, compounds A, B, and C are coumarin-based derivatives designed to inhibit the urease enzyme [22–24]. In addition to coumarin, triazole ring is a notable pharmacophore in drug development specially urease inhibitors [25–29]. Compounds D, E, and F (Fig. 1) were designed based on a triazole pharmacophore aimed at inhibiting urease [30–32]. In this study, novel coumarin-based acetohydrazide-1,2,3-triazole derivatives were designed and synthesized by connecting the two main rings triazole and coumarin through Schiff base bonds [33], positioning them as promising urease inhibitors.

2. Results and discussion

2.1. Chemistry

In the first phase, the synthesis of 5-hydroxy-4,7-dimethyl-2*H*-chromen-2-one (**3**) was achieved by reacting 5-methylbenzene-1,3-diol (**2**) with ethyl acetoacetate (**1**) in the presence of polyphosphoric acid as a catalyst [34]. The reaction proceeded under solvent-free conditions at 70–80 °C for 30 min. Subsequent reaction of compound (**3**) with ethyl 2-bromoacetate (**5**) and K_2CO_3 in DMF at room temperature yielded ethyl 2-((4,7-dimethyl-2-oxo-2*H*-chromen-5-yl)oxy)acetate (**6**) after 8 h [35]. Transformation of compound (**6**) to 2-((4,7-dimethyl-2-oxo-2*H*-chromen-5-yl)oxy)acetohydrazide (**7**) was performed using hydrazine hydrate in ethanol under reflux for 12 h [36].

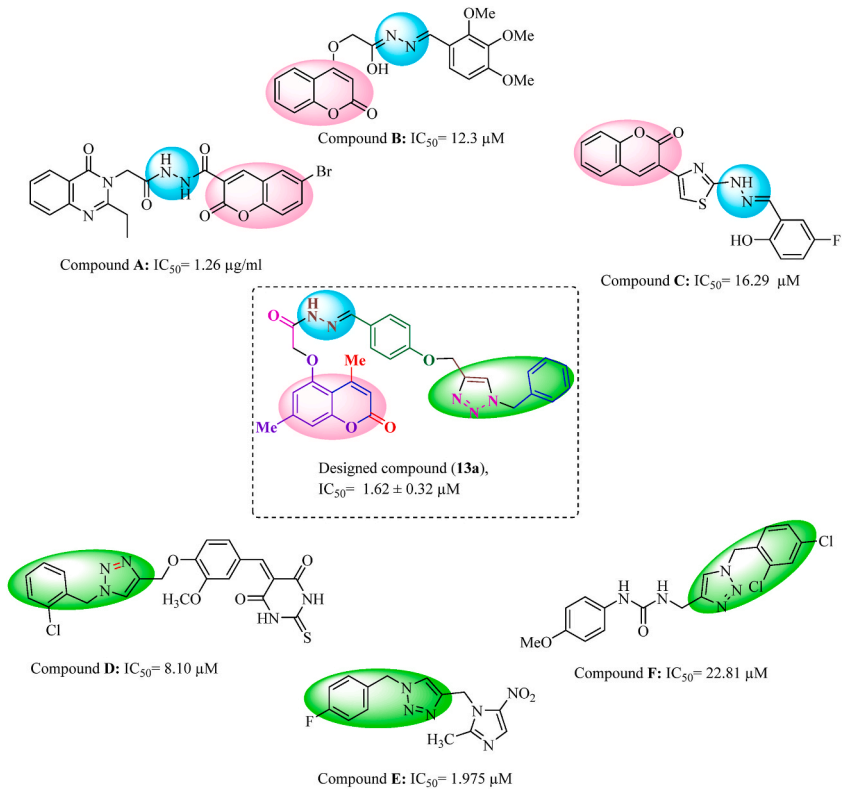

Fig. 1. Chemical structures of some urease enzyme inhibitors based on coumarin-based acetohydrazide-1,2,3-triazole derivatives.

In the second phase, the synthesis of triazole based benzaldehyde derivatives (**12a-12o**) was carried out. Initially, the reaction of 3-hydroxy, 4-hydroxy, or 3-methoxy-4-hydroxy benzaldehyde derivatives (**8a-8c**) with 3-bromoprop-1-yne (propargyl bromide) in the presence of K_2CO_3 in acetone produced propargylated hydroxy benzaldehydes (**9a-9o**). Subsequently, benzyl halide derivatives (**10a-10e**) were reacted with NaN_3 in DMF to yield benzyl azide derivatives (**11a-11e**). In the next step, propargylated hydroxy benzaldehydes (**9a-9o**) were subjected to the benzyl azide derivatives (**11a-11e**) in a click reaction, utilizing ascorbic acid and $CuSO_4{\cdot}5H_2O$ as

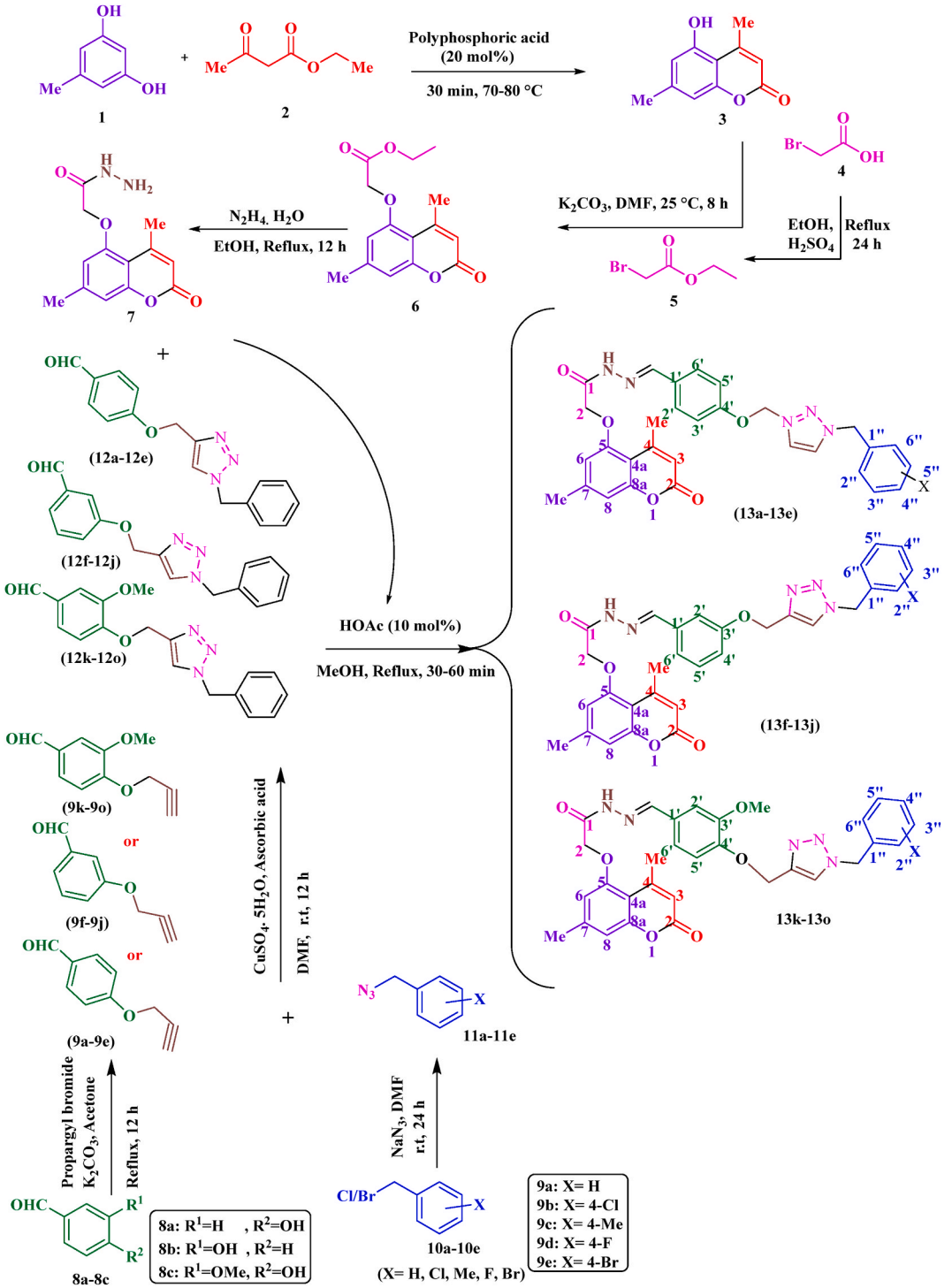

Scheme 1. Synthesis of novel coumarin-based acetohydrazide-1,2,3-triazole derivatives.

catalysts, which resulted in the formation of the desired triazole base aldehyde derivatives (**12a-12o**) [37].

In the final phase, acetohydrazide derivatives based on triazole and coumarin moieties (**13a-13o**) were synthesized by reacting compound (**7**) with the triazole base aldehyde derivatives (**12a-12o**) in methanol under reflux with HOAc (10 %) as a catalyst [38]. The resulting white solids were isolated, dried, and the structures of all target synthesized compounds (**13a-13o**) were confirmed using ^{1}H NMR, ^{13}C NMR, mass spectrometry, elemental analysis, and IR spectroscopy (see Scheme 1).

2.2. Biological study

2.2.1. In vitro urease inhibitory activity

The target products were assessed for their *in vitro* anti-urease activity and compared to the standard thiourea (Table 1). The synthesized compounds are divided into three groups based on the linker: 1) **13a-13e** with para-substituted phenylene rings, 2) **13f-13j** with meta-substituted phenylene rings, and 3) **13k-13o** with para-substituted 3-methoxyphenylene rings. Among the synthesized compounds, compound **13a** exhibited the highest urease inhibitory activity with an IC_{50} value of 1.62 ± 0.32 μM. Other compounds also showed significant activity with IC_{50} values ranging from 3.584 ± 0.91 μM for compound **13c** to 16.91 ± 0.68 μM for compound **13d**. The standard inhibitor, thiourea, displayed an IC_{50} value of 23.11 ± 1.02 μM.

Comparison of compounds **13a-13e** revealed that the compound **13a** with unsubstituted benzyl ring (X = H) showed the highest inhibitory activity (1.619 ± 1.02 μM). The fluorine substituent in compound **13d** led to lower activity (16.91 ± 0.68 μM), possibly due to the high electronegativity of fluorine affecting binding interactions. The presence of a chlorine atom at the 4-position for compound **13b** increased activity (7.496 ± 0.54 μM). The electron-withdrawing effect of chlorine is less than that of fluorine, but it has higher lipophilicity. The presence of bromine substitution at the 4-position in compound **13e** resulted in decreased inhibitory activity (11.77 ± 1.32 μM). This decrease in activity could be attributed to steric hindrance within the active site. Substitution with a methyl group at the 4-position of the benzyl moiety in compound **13c** enhanced activity compared to halogen substitutions (3.584 ± 0.91 μM), indicating that the electron-donating effect of the methyl group may facilitate more favorable interactions with urease compared to halogens. As a result, substitutions at the para position of the benzyl moiety in compounds **13a-13e** did not enhance inhibitory activity.

For compounds **13f-13j**, compound **13f** with an unsubstituted benzyl ring (X = H) exhibited the highest inhibitory activity (7.927 ± 0.98 μM), suggesting that the absence of substituents in the benzyl moiety may enhance interactions with the urease enzyme due to reduced steric effects. Compound **13i**, with a 4-fluorine substituent, caused a minor decrease in inhibitory activity (8.415 ± 0.53 μM), while the presence of a chlorine atom at the 4-position in compound **13g** resulted in a slightly greater decrease in activity to 9.59 ± 1.67 μM. Compound **13j** with bromine substitution at the 4-position led to further decreased inhibitory activity (11.77 ± 1.32 μM). Substitution with a methyl group at the 4-position in compound **13h** resulted in significant decreased in activity (14.29 ± 2.15 μM). Overall, compounds **13f-13j** did not demonstrate a significant role in urease inhibitory activity.

In compounds **13k-13o**, the addition of a methoxy group at the 3-position of the phenylene linker, as an electron-donating group, increased the electron density of the middle ring but also introduced steric hindrance. Compound **13k**, with an unsubstituted benzyl moiety, exhibited decreased inhibitory activity (14.83 ± 1.02 μM) compared to its corresponding compounds **13f** and **13a**. Substitution with chlorine in compound **13l** resulted in a minor improvement in inhibitory activity (13.17 ± 2.06 μM). The electronegativity and hydrophobic nature of chlorine likely contributed to better binding interactions with the enzyme, although the overall improvement was minimal. The presence of a bromine substitution in compound **13o** further enhanced inhibitory activity, resulting in an IC_{50} of 11.16 ± 0.50 μM. Fluorine substitution in compound 13n led to the best activity within the halogen series likely due to its strong electronegativity, with an with an IC_{50} value of 10.29 ± 1.09 μM. Substitution with a methyl group in compound **13m** showed a significant improvement in inhibitory effect (8.117 ± 1.12 μM), possibly due to the hydrophobicity character of the methyl as electron donating group. In summary, for compounds **13k-13o**, which contain a methoxy group at the 3-position of the phenylene middle ring, steric hindrance from the methoxy group and conformational changes compared to their corresponding compounds **13a-13e**

Table 1
Inhibitory activities of the new compounds **13a-13o** against urease enzyme.

Entry	Compounds	X	IC_{50} (μM) ± SE[a]
1	**13a**	H	1.620 ± 0.32
2	**13b**	4-Cl	7.496 ± 0.54
3	**13c**	4-Me	3.584 ± 0.91
4	**13d**	4-F	16.91 ± 0.68
5	**13e**	4-Br	11.77 ± 1.32
6	**13f**	H	7.927 ± 0.98
7	**13g**	4-Cl	9.591 ± 1.67
8	**13h**	4-Me	14.29 ± 2.15
9	**13i**	4-F	8.415 ± 0.53
10	**13j**	4-Br	10.08 ± 0.28
11	**13k**	H	14.83 ± 1.02
12	**13l**	4-Cl	13.17 ± 2.06
13	**13m**	4-Me	8.117 ± 1.12
14	**13n**	4-F	10.29 ± 1.09
15	**13o**	4-Br	11.16 ± 0.50
16	**Thiourea**		23.11 ± 1.02

decreased urease inhibitory activity.

2.2.2. Kinetic study

A kinetic study of the active compound **13a** against urease was conducted to elucidate the inhibition mechanism. The Lineweaver-Burk plot, illustrated in Fig. 2a, shows that increasing concentrations of compound **13a** lead to a proportional decrease in both Vmax and Km. This observation indicates that compound **13a** acts as an uncompetitive inhibitor of urease. Uncompetitive inhibitors are a specific type of enzyme inhibitor that bind exclusively to the enzyme-substrate complex (E-S complex), preventing the conversion of the substrate into product. As illustrated in Fig. 2b, the inhibition constant (Ki) was calculated by plotting 1/Vmax against the concentrations of inhibitor **13a**, resulting in a Ki value of 1.99 μM. This Ki value highlights the potency of compound **13a** as an effective inhibitor of urease.

2.2.3. Molecular docking study

The active site of Urease from Jack Bean (JBU) is composed of twelve key amino acids, which include bi-nickel ions, His407, His409, Lys490, His492, Asp494, His519, His545, Cys592, His593, Arg609, Asp633, and Ala636 [39]. The Most ureases contain conserved residues that form a mobile flap, which serves to cover the active site [40]. In JBU, the residues comprising the mobile flap are 590–609 as a part of helix-turn-helix structure [39]. The flap is thought to act as a gate controlling access to the active site with conformation change from a closed state to an open state to allow substrate entry and product release [41]. The flap residues play a critical role in urease inhibition because they contribute to the flexibility of the mobile flap that covers the entrance to the active site. Inhibitors that bind to these residues or alter their interactions can reduce the flap's flexibility.

According to the molecular docking results, hydrogen bonding and metal chelation are two important pharmacophoric interactions. Figs. 3 and 4 (Time 0) shows the initial position of **13a** in the active site of urease as predicted by molecular docking. The estimated free energy of binding, which is defined as the total sum of final intermolecular energy, final total internal energy, and torsional free energy minus the unbound system's energy, is calculated to be −7.99 kcal/mol. The coumarin moiety of **13a** forms a hydrogen bond with His492 and van der Waals (vdW) interactions with His593 and His545. Furthermore, this privileged heterocycle participates in two π-cation interactions with Arg609 and Asp494, as well as metal chelation through its carbonyl group. The hydrogen bond between the carbonyl moiety of 13a and His492, along with metal chelation by the carbonyl moiety, and the rigid structure of the hydrazine group in **13a**, result in the most energetically favorable conformation of the ligand within the urease binding pocket. To evaluate the stability of the predicted complex, a molecular dynamics (MD) simulation was carried out.

2.2.4. Molecular dynamics

Considering the compatibility of the urease enzyme with our applied force field (CHARMM36), a 20 ns MD run was conducted to assess the stability of the nickel ions within the binding site. Our findings revealed that the nickel ions settled within the binding site and were chelated by surrounding histidine residues (His407, His409, His519, and His545).

To evaluate the stability of the predicted docking pose of **13a**, a 100 ns MD simulation was conducted (Fig. 3). The temperature and total energy fluctuations remained stable, with an average temperature of 300.0 K indicating a well-equilibrated system. The system's energy showed only a 0.11 % RSD over 100 ns, demonstrating energy conservation. Despite initial fluctuations (red regions in the RMSD matrix) caused by induced-fit between **13a** and the active site residues, the system eventually reached an equilibrium state (yellow-blue region in the RMSD matrix). The coordination and positions of the Ni ions in the binding site remained relatively consistent, which is crucial for maintaining the integrity of the active site for binding functions. Hydrogen bonding interactions also played an important role in stabilizing and properly orienting the ligand in the enzyme's active site.

The impact of ligand binding on urease was assessed through analyzing the radius of gyration (R_g) (mean = 3.08 with an RSD of 0.40 %). Based on the obtained results, it was observed a contraction in the structure of the **13a**-urease complex from 5 ns to 30 ns. During this period, the ligand experienced conformational changes leading to a more stable complex (See ligand RMSD matrix, Fig. 3). At the beginning of the simulation, **13a** via its coumarin moiety formed chelating interactions with nickel ions (Figs. 3 and 4, time 0 ns). However, at 18 ns, **13a** started to rotate by 90° from its initial position. This rotation led to the dissociation of the coumarin moiety from the nickel ions, prompting it to approach the SER579-HIS593 α-helix (Fig. 3, time 18 ns). At the same time, the pocket that accommodated the coumarin moiety expanded as a result of the movement of the Pro600-Arg609 α-helix of mobile flap motif. As the simulation progressed to 37 ns, the position of the benzyl moiety, attached to hydrazine and the triazole ring, changed. This change led

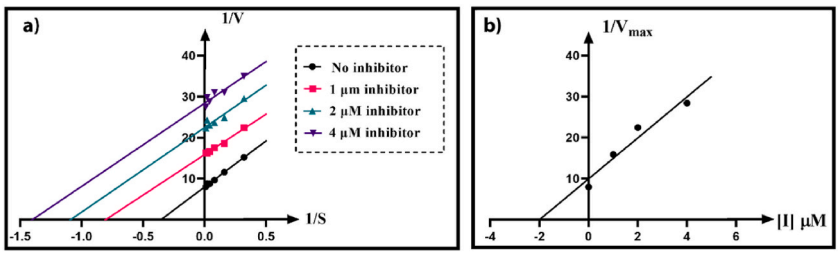

Fig. 2. Kinetic study of compound **13a** against urease. (a) The Lineweaver– Burk plot in the absence and presence of different concentrations of compound **13a**; (b) The secondary plot between K_m and various concentrations of compound **13a**.

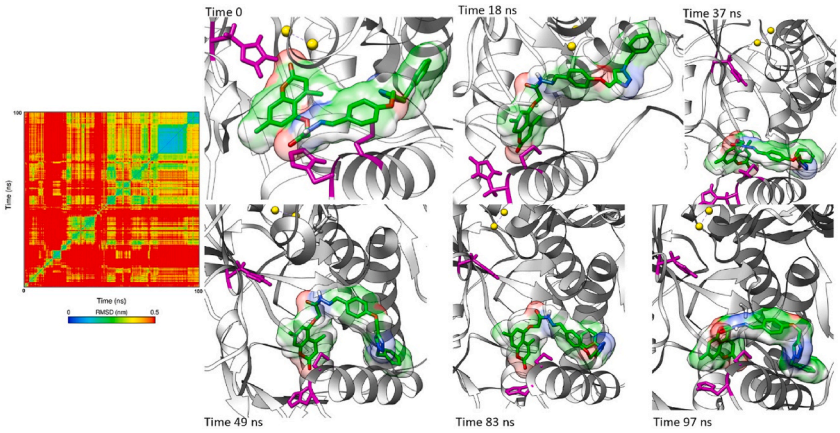

Fig. 3. RMSD matrix and selected trajectories of compound **13a** during 100 ns MD simulation. The enzyme is showed in flat ribbon style. The enzyme is showed in gray color, the nickel ions are showed in yellow color, the key residues of active site are showed in purple color and the ligand is showed in green color.

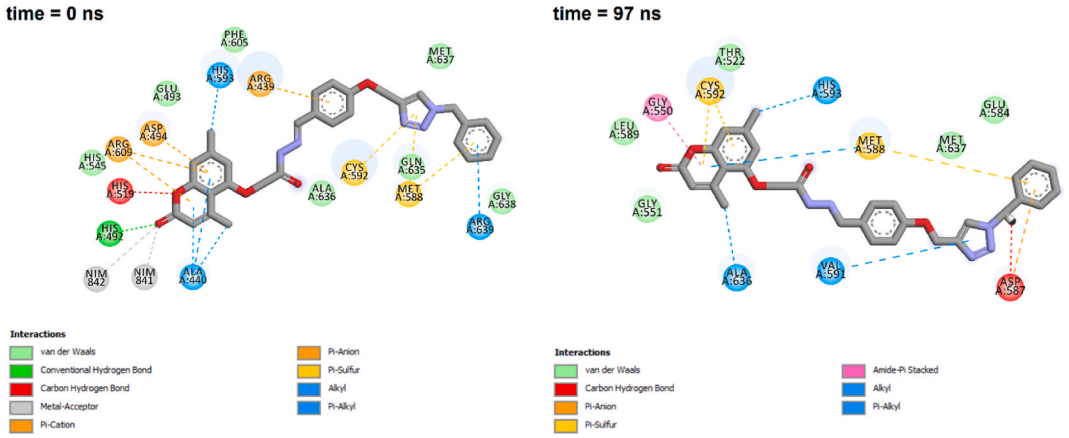

Fig. 4. 2D presentation of interactions of compound **13a** at time 0 ns (initial docking pose) and time 97 ns (after equilibration).

to a bent conformation of **13a**, interacting with both sides of the SER579-HIS593. The new U-shape conformer of **13a** changed in the way nickel ions chelated to the surrounding His residues. By 97 ns, **13a**, along with the nickel ions and surrounding α-helix, reached a stable configuration, indicative of equilibrium within the active site entrance (Figs. 3 and 4, Time 97 ns). As shown in Fig. 5, the conformational changes of the enzyme-inhibitor complexes are depicted at 0 ns and 97 ns. At 97 ns, it can be observed that the nickel ions and the α-helix, including the Pro600-Arg609 residues of the mobile flap at the entrance of the active site, have moved further apart compared to their positions at 0 ns. The inhibitor interacts with the flap motif, while the nickel ions in the active site do not directly interact with the inhibitor. In the course of the molecular dynamics (MD) simulation, critical interactions between the ligand **13a** and key residues of the urease active site were observed. Notably, at 18 ns, a π-alkyl interaction was formed between the coumarin moiety of **13a** and Cys592, which played a role in stabilizing the ligand within the active site. As the simulation progressed a π-sulfur interaction formed between the coumarin moiety and Cys592 at 37 ns. By 49 ns, both π-sulfur and π-alkyl interactions between the coumarin moiety and Cys592 were established, suggesting increased stability. This dual interaction persisted through 83 ns, further confirming the role of Cys592 in maintaining the ligand's conformation. At 97 ns, the π-sulfur interaction with Cys592 was retained, while a new π-alkyl interaction between the methyl group attached to the coumarin moiety and His593 emerged, indicating a final stable conformation of the ligand in the binding site. These interactions highlight the dynamic nature of **13a**'s binding mode and its adaptability to key residues within the active site, particularly Cys592 and His593, which appear to be crucial for maintaining the ligand's stable positioning during the simulation.

The molecular dynamics simulation results reveal that the **13a** tends to remain near the SER579-HIS593 α-helix rather than nickel ions, which are crucial for catalytic activity of urease, within the active site, leading to keep opening the upper part of the active site, which is responsible for substrate binding. This interaction suggests that the **13a** causes a conformational change in the active site which supports uncompetitive inhibition. In other words, the molecular dynamics simulation results suggest that **13a** can bind to the substrate-enzyme complex and form a ternary complex. These findings confirmed the proposed mechanism of action for **13a** as an

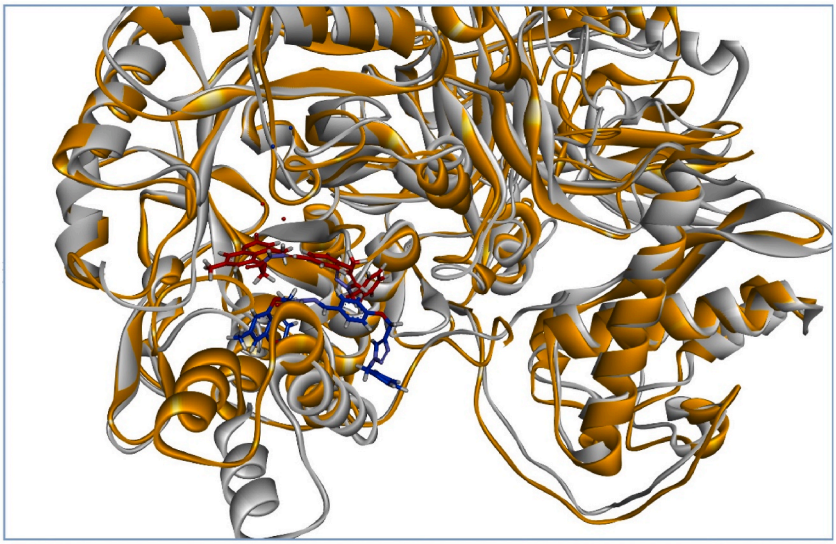

Fig. 5. Comparison of enzyme-inhibitor complex at time 0 ns (red/orange color) and time 97 ns (blue/gray color).

uncompetitive inhibitor.

The total root mean square fluctuation (RMSF) of both the **13a**-urease complex and the apo enzyme (3LA4) is depicted in Fig. 6. The difference in RMSF between the *apo* and *holo* structures exceeded 0.1 nm in only a few residues. Residues within the range of 490–610, including five crucial amino acids in the active site (His492, Asp494, Cys592, His593, and Arg609), experienced high fluctuation in RMSF, up to 0.15 nm. As explained above, RMSF confirmed that the metal chelating between **13a** and Ni atoms was not stable during the MD simulation. The RMSF of residues surrounding the Ni atoms decreased during the MD simulation, indicating a stronger interaction between His residues and Ni atoms. These results can improve our understanding of fundamental molecular interactions and help us design novel inhibitors with enhanced binding capabilities in various research contexts.

2.2.5. Prediction of ADMET properties

The pkCSM and SwissADME online servers were used to calculate ADMET parameters (28, 29). The synthesized compounds **13a**-**13o** were evaluated using these servers to predict their pharmacokinetic profiles and potential safety issues, with the results illustrated in Table 2 [42,43].The absorption data indicates high intestinal absorption across all compounds, ranging from 93.414 % to 100 %, suggesting efficient uptake from the gastrointestinal tract. Distribution predictions revealed poor blood-brain barrier (BBB) permeability, with negative scores ranging from −1.027 to −1.552, indicating low potential for central nervous system (CNS) exposure, which is favorable for avoiding CNS-related side effects. The CNS permeability scores were also low for all compounds.

In terms of metabolism, none of the compounds were predicted to inhibit the CYP1A2 enzyme, which is involved in drug

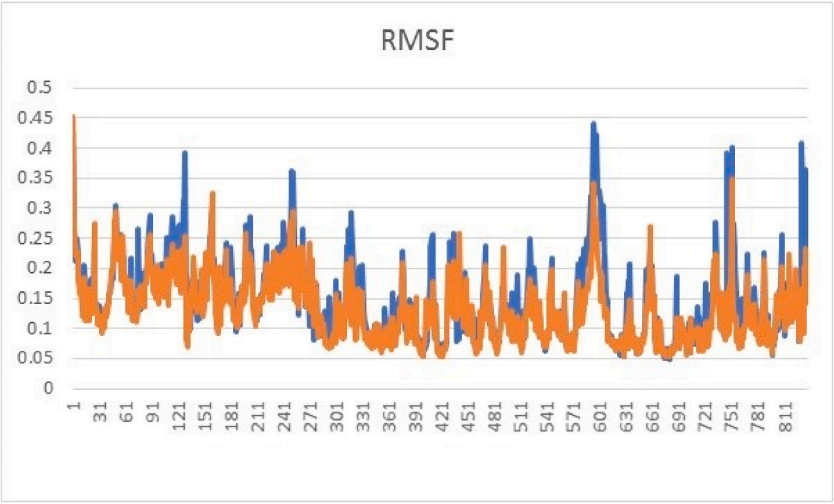

Fig. 6. RMSF Analysis of **13a**-urease complex (blue) vs. apo enzyme (orange).

Table 2
ADMET prediction of the compounds **13a-13o**.

compound	Absorption	Distribution		Metabolism					Excretion	Toxicity	
	Intestinal absorption (%Absorbed)	BBB permeability	CNS permeability	CYP1A2 inhibitior	CYP2C19 inhibitior	CYP2C9 inhibitior	CYP2D6 inhibitior	CYP3A4 inhibitior	Renal OCT2 substrate	AMES toxicity	hERG I inhibitor
13a	93.414	−1.313	−3.083	No	Yes	Yes	No	Yes	No	No	No
13b	94.633	−1.501	−3.023	No	Yes	Yes	No	Yes	No	No	No
13c	100	−1.391	−3.209	No	Yes	Yes	No	Yes	No	No	No
13d	94.674	−1.533	−3.215	No	Yes	Yes	No	Yes	No	No	No
13e	94.369	−1.509	−3.01	No	Yes	Yes	No	Yes	No	No	No
13f	96.233	−1.331	−3.09	No	Yes	Yes	No	Yes	No	No	No
13g	97.451	−1.519	−3.03	No	Yes	Yes	No	Yes	No	No	No
13h	97.939	−1.027	−3.221	No	Yes	Yes	No	Yes	No	No	No
13i	97.492	−1.552	−3.222	No	Yes	Yes	No	Yes	No	No	No
13j	97.187	−1.528	−3.016	No	Yes	Yes	No	Yes	No	No	No
13k	95.516	−1.238	−3.492	No	Yes	Yes	No	Yes	No	No	No
13l	96.735	−1.408	−3.432	No	Yes	Yes	No	Yes	No	No	No
13m	96.027	−1.233	−3.444	No	Yes	Yes	No	Yes	No	No	No
13n	96.776	−1.441	−3.616	No	Yes	Yes	No	Yes	No	No	No
13o	96.471	−1.416	−3.419	No	Yes	Yes	No	Yes	No	No	No

metabolism. However, all compounds were predicted to inhibit CYP2C19, CYP2C9, and CYP3A4 enzymes, indicating potential for drug-drug interactions with other medications metabolized by these pathways. Importantly, none of the compounds showed inhibition of CYP2D6, suggesting a more selective metabolic profile. Excretion predictions indicated that none of the compounds were substrates for renal OCT2.

Toxicity predictions for the all compounds were promising, with no compounds showing signs of AMES toxicity, suggesting a low likelihood of mutagenic effects. Additionally, none of the compounds were predicted to inhibit hERG channels, which are associated with cardiotoxicity, indicating a low risk of adverse cardiac effects. Overall, these ADMET predictions highlight the favorable pharmacokinetic and safety profiles of compounds **13a-13o**, making them promising candidates for further development as therapeutic agents.

3. Conclusion

In this study, a series of novel coumarin-based acetohydrazide-1,2,3-triazole derivatives were designed, synthesized, and evaluated as urease enzyme inhibitors. All compounds indicated significant inhibitory activity, notably compound **13a**, which exhibited the highest activity with an IC_{50} value of 1.619 ± 0.32 μM compared to the standard inhibitor, thiourea. The structure-activity relationship (SAR) analysis indicated that the nature and position of substituents on the benzyl moiety do not play a significant role in modulating urease inhibitory activity. Kinetic studies confirmed that compound **13a** acts as an uncompetitive inhibitor of urease, with a *Ki* value of 1.99 μM. Based on *in silico* studies, the coumarin moiety of compound **13a** through hydrogen bonding and metal-chelation interactions, and the hydrazine group through its rigid structure contributed to the most favorable binding conformation. MD simulations indicated that the nickel ions and the flap at the entrance of the catalytic site moved away from each other and the stable conformation of **13a** interacted solely with the flap (helix-turn-helix motif) through interactions with Ser579-His593 at entrance of active site without any interaction with nickel. Consequently, all *in vitro* and *in silico* results suggest that compound **13a** inhibits urease activity as an uncompetitive inhibitor by stabilizing the active site flap. Thus, novel coumarin-based acetohydrazide-1,2,3-triazole derivatives could serve as promising agents for developing novel therapeutic compounds with acceptable pharmacokinetic properties and low toxicity for treating urease-associated diseases, such as *H*. pylori infections.

4. Experimental

All chemicals were sourced from Merck and Aldrich. NMR (^{1}H and ^{13}C) and IR spectra were recorded using a Bruker 400-NMR and ALPHA FT-IR spectrometer on KBr disks, respectively. Mass spectrometry (MS) data were obtained from an Agilent Technologies (HP) mass spectrometer operating at an ionization potential of 70 eV. Elemental analysis was performed using an Elementar Analysensystem GmbH VarioEL CHNS model. Chemical shifts (δ) and coupling constants (J) were reported in parts per million (ppm) and Hertz, respectively. The atom numbering of the target compounds, based on their IUPAC names, was used to assign the ^{1}H NMR data. The original spectra of the investigated compounds are provided as Supporting Information Data.

4.1. Chemistry

General procedure for the synthesis of 5-hydroxy-4,7-dimethyl-2*H*-chromen-2-one) 3)

According to the previously reported procedure [34], 5-methylbenzene-1,3-diol**)2)** (5 mmol) and ethyl acetoacetate**) 1)** (5 mmol) were added into a 50 mL round-bottom flask. Then, polyphosphoric acid (20 mol%) was added as a catalyst. The reaction mixture was placed at 80-70 °C for 30 min under solvent-free conditions. Progress of the reaction was followed by applying of TLC technique (EtOAc: *n*-Hexane; 1:1). At the end of the reaction, 30 mL of water was added to the reaction mixture and placed on the stirrer for 10 min. The resulting precipitate is filtered and washed twice with water. The resulting yellow precipitate was dried at 80 °C for 2 h (Mp: 240–242 °C).

General method for the synthesis of ethyl 2-((4,7-dimethyl-2-oxo-2*H*-chromen-5-yl)oxy)acetate) 6)

After synthesis of 5-hydroxy-4,7-dimethyl-2*H*-chromen-2-one**) 3)**, in a 50 mL round-bottomed flask, a mixture of 5-hydroxy-4,7-dimethyl-2*H*-chromen-2-one**) 3)** (5 mmol), ethyl 2-bromoacetate**) 5)** (5 mmol) which was obtained according to previously reported and K_2CO_3 (5 mmol) were placed in DMF (10 mL) as solvent at 25 °C for 8 h [35]. Progress of the reaction was followed by applying of TLC technique (EtOAc:*n*-Hexane; 2:1). At the end of the reaction, 30 mL of water was added to the reaction mixture and placed on the stirrer for 10 min. The resulting precipitate is filtered and washed several times with water. The resulting white solid was placed to dry at 100 °C for 3 h (Mp: 167–170 °C).

General method for the synthesis of 2-((4,7-dimethyl-2-oxo-2*H*-chromen-5-yl)oxy)acetohydrazide) 7)

After synthesis of ethyl 2-((4,7-dimethyl-2-oxo-2*H*-chromen-5-yl)oxy)acetate) **6**), a mixture of ethyl 2-((4,7-dimethyl-2-oxo-2*H*-chromen-5-yl)oxy)acetate) **6**) (5 mmol), N_2H_4, H_2O (10 mmol), and ethanol (30 mL) were added into a 50 mL round-bottom flask and placed under refluxed condition for 12 h [36]. Progress of the reaction was followed by applying of TLC technique (EtOAc:*n*-Hexane; 2:1). At the end of the reaction, the resulting precipitate was filtered and washed several times with ethanol. The resulting white solid was placed to dry at 80 °C for 5 h (Mp: 234–236 °C).

General method for the synthesis of triazole based benzaldehyde derivatives) 12a-12o)

A mixture of hydroxy benzaldehyde derivatives)3-hydroxy-benzaldehde, 4-hydroxy-benzaldehde, 3-methoxy-4-hydroxy-benzaldehde) (**8a-8c**) (5 mmol), 3-bromoprop-1-yne or propargyl bromide (6 mmol) and K_2CO_3 (5 mmol) were placed in acetone as solvent (30 mL) for 12 h under reflux condition. After the completion of the reaction, the reaction solution was evaporated after filtration to

isolate K_2CO_3, and the remaining precipitate was washed several times with a mixture of ethyl acetate and *n*-hexane to obtain propargylated aldehydes (**9a-9o**). On the other side, conversion of benzyl halide derivatives (**10a-10o**) to benzyl azide derivatives (**11a-11e**) was performed by stirring derivatives (**10a-10o**) (2 mmol) and NaN_3 (3 mmol) in DMF (5 mL) at 25 °C for 24 h. The obtained mixture containing benzyl azide derivatives (**11a-11o**) in DMF (1.5 mmol) was directly subjected to ascorbic acid (10 mol%), $CuSO_4{\cdot}5H_2O$ (10 mol%), and propargylated aldehydes (**9a-9o**), and then stirred for 24 h at 25 °C. After the completion of the reaction (checked by TLC), 50 mL of ammonia solution (H_2O:NH_3; 49:1) and EtOAc were added to the reaction mixture and decanted. The organic layer was separated and Na_2SO_4 was added to the reaction mixture to remove excess H_2O. The organic layer was evaporated to obtain triazole based benzaldehyde derivatives (**12a-12o**) [37].

General method for the synthesis of coumarin-based acetohydrazide-1,2,3-triazole derivatives (13a-13o)

In a 25 mL round-bottomed flask, a mixture of 2-((4,7-dimethyl-2-oxo-2*H*-chromen-5-yl)oxy)acetohydrazide) **7**) (0.5 mmol), triazole based benzaldehyde derivatives (**12a-12o**) (0.6 mmol), MeOH (15 mL), and HOAc (10 mol%) as a catalyst was placed in under refluxing condition. Progress of the reaction was followed by applying of TLC technique (EtOAc: n-Hexane (4:1)). At the end of the reaction, the resulting precipitate was filtered and washed several times with hot MeOH [38].

(E)-N'-(4-((1-Benzyl-1H-1,2,3-triazol-4-yl)methoxy)benzylidene)-2-((4,7-dimethyl-2-oxo-2H-chromen-5-yl)oxy)acetohydrazide (13a).

White solid; Yield 90 %; Mp: 240–242 °C; IR (KBr, cm^{-1}): 3241, 17.22, 1696, 1123. ^{1}H NMR (400 MHz, DMSO-d_6) δ (ppm): 11.56 (s, 1H, NH), 8.33 (s, 1H, H (Imine)), 7.97 (s, 1H, H (triazole)), 7.67 (d, J = 8.2 Hz, 2H, $H_{2'}$, $H_{6'}$), 7.40–7.32 (m, 5H, Benzyl), 7.10 (d, J = 8.2 Hz, 2H, $H_{3'}$, $H_{5'}$), 6.86–6.76 (m, 2H, H_6, H_8), 6.14 (s, 1H, H_3), 5.63 (s, 2H, CH_2), 5.28 (s, 2H, CH_2), 5.20 (s, 2H, CH_2), 2.63 (s, 3H, CH_3 (7)), 2.35 (s, 3H, CH_3 (4)). ^{13}C NMR (100 MHz, DMSO-d_6) δ (ppm): 168.1, 163.3, 159.5, 159.4, 156.5, 154.5, 154.3, 143.7, 143.0, 135.9, 128.7, 128.5, 128.1, 127.9, 126.7, 124.8, 114.9, 113.0, 112.8, 110.1, 109.6, 108.9, 107.8, 65.8, 61.1, 52.8, 23.8, 21.3. Anal. calcd. for $C_{30}H_{27}N_5O_5$: C, 67.03; H, 5.06; N, 13.03. Found: C, 67.11; H, 4.97; N, 13.09. MS: *m/z* (%); 537.4 (M^+, 3.3), 520.3 (2.1).

(E)-N'-(4-((1-(4-Chlorobenzyl)-1H-1,2,3-triazol-4-yl)methoxy)benzylidene)-2-((4,7-dimethyl-2-oxo-2H-chromen-5-yl)oxy)acetohydrazide (13b).

White solid; Yield 85 %; Mp: 229–231 °C; IR (KBr, cm^{-1}): 3419, 1731, 1696, 1125. ^{1}H NMR (400 MHz, DMSO-d_6) δ (ppm): 11.56 (s, 1H, NH), 8.33 (s, 1H, H (Imine)), 7.98 (s, 1H, H (triazole)), 7.68 (d, J = 7.6 Hz, 2H, $H_{2'}$, $H_{6'}$), 7.46 (d, J = 4.9 Hz, 2H, $H_{3''}$, $H_{5''}$), 7.36 (d, J = 4.9 Hz, 2H, $H_{2''}$, $H_{6''}$), 7.12 (d, J = 7.6 Hz, 2H, $H_{3'}$, $H_{5'}$), 6.87–6.77 (m, 2H, H_6, H_8), 6.15 (s, 1H, H_3), 5.64 (s, 2H, CH_2), 5.29 (s, 2H, CH_2), 5.21 (s, 2H, CH_2), 2.63 (s, 3H, CH_3 (7)), 2.36 (s, 3H, CH_3 (4)). ^{13}C NMR (100 MHz, DMSO-d_6) δ (ppm): 168.6, 160.0, 159.9, 157.1, 155.0, 154.8, 144.3, 143.5, 143.2, 135.4, 133.3, 130.4, 129.2, 127.3, 125.3, 115.5, 113.3, 110.1, 109.5, 108.3, 66.3, 61.6, 52.5, 24.4, 21.8. Anal. calcd. for $C_{30}H_{26}ClN_5O_5$: C, 62.99; H, 4.58; N, 12.24. Found: C, 62.93; H, 4.60; N, 12.19.

(E)-2-((4,7-Dimethyl-2-oxo-2H-chromen-5-yl)oxy)-N'-(4-((1-(4-methylbenzyl)-1H-1,2,3-triazol-4-yl)methoxy)benzylidene)acetohydrazide (13c).

White solid; Yield 87 %; Mp: 240–242 °C; IR (KBr, cm^{-1}): 3318, 2935, 1728, 1693, 1438, 1130. ^{1}H NMR (400 MHz, DMSO-d_6) δ (ppm): 11.57 (s, 1H, NH), 8.30 (s, 1H, H (Imine)), 7.99 (s, 1H, H (triazole)), 7.68 (d, J = 6.3, 2H, $H_{2'}$, $H_{6'}$), 7.25 (d, J = 8.2 Hz, 2H, $H_{3''}$, $H_{5''}$), 7.20 (d, J = 8.2 Hz, 2H, $H_{2''}$, $H_{6''}$), 7.12 (d, J = 6.3, 2H, $H_{3'}$, $H_{5'}$), 6.88–6.78 (m, 2H, H_6, H_8), 6.17 (s, 1H, H_3), 5.57 (s, 2H, CH_2), 5.30 (s, 2H, CH_2), 5.20 (s, 2H, CH_2), 2.64 (s, 3H, CH_3 (7)), 2.38 (s, 3H, CH_3 (4)), 2.30 (s, 3H, CH_3 (4")). ^{13}C NMR (100 MHz, DMSO-d_6) δ (ppm): 168.7, 160.1, 157.1, 155.1, 154.8, 148.0, 144.3, 143.5, 143.1, 138.4, 133.4, 129.7, 129.0, 128.5, 127.3, 125.1, 115.5, 113.3, 110.6, 110.2, 109.5, 66.3, 61.7, 53.1, 24.4, 21.9, 21.1. Anal. calcd. for $C_{31}H_{29}N_5O_5$: C, 67.50; H, 5.30; N, 12.70. Found: C, 67.43; H, 5.27; N, 12.69. MS: *m/z* (%); 551.7 (M^+, 1.6), 441.4 (5.8), 368.4 (7.8), 236.3 (13.1), 171.1 (13.2), 129.1 (21), 105.1 (26.3), 83.2 (47.3), 57.2 (100).

(E)-2-((4,7-Dimethyl-2-oxo-2H-chromen-5-yl)oxy)-N'-(4-((1-(4-fluorobenzyl)-1H-1,2,3-triazol-4-yl)methoxy)benzylidene)acetohydrazide (13d).

White solid; Yield 80 %; Mp: 260–262 °C; IR (KBr, cm^{-1}): 3244, 1725, 1694, 1122. ^{1}H NMR (400 MHz, DMSO-d_6) δ (ppm): 11.57 (s, 1H, NH), 8.33 (s, 1H, H (Imine)), 7.99 (s, 1H, H (triazole)), 7.68 (d, J = 6.4 Hz, 2H, $H_{2'}$, $H_{6'}$), 7.46–7.41 (m, 2H, $H_{3''}$, $H_{5''}$), 7.27–7.22 (m, 2H, $H_{2''}$, $H_{6''}$), 7.14–7.10 (d, J = 6.4 Hz, 2H, $H_{3'}$, $H_{5'}$), 6.88–6.79 (m, 2H, H_6, H_8), 6.17 (s, 1H, H_3), 5.63 (s, 2H, CH_2), 5.30 (s, 2H, CH_2), 5.20 (s, 2H, CH_2), 2.65 (s, 3H, CH_3 (7)), 2.37 (s, 3H, CH_3 (4)). ^{13}C NMR (100 MHz, DMSO-d_6) δ (ppm): 168.8, 159.8, 157.1, 154.8, 151.2, 148.1, 144.0, 143.2, 139.3, 132.7, 130.9, 130.7, 129.0, 125.2, 122.0, 116.25, 115.9, 115.5, 113.4, 110.2, 109.5, 67.7, 61.6, 52.5, 24.3, 21.8. Anal. calcd. for $C_{30}H_{26}FN_5O_5$: C, 67.03; H, 5.06; N, 13.03. Anal. calcd. for $C_{30}H_{26}FN_5O_5$: C, 64.86; H, 4.72; N, 12.61. Found: C, 64.93; H, 4.70; N, 12.69. MS: *m/z* (%); 555.3 (M^+, 0.6), 366.2 (5.8), 190.1 (23.5), 162.1 (50.1), 109.1 (100).

(E)-N'-(4-((1-(4-Bromobenzyl)-1H-1,2,3-triazol-4-yl)methoxy)benzylidene)-2-((4,7-dimethyl-2-oxo-2H-chromen-5-yl)oxy)acetohydrazide (13e).

White solid; Yield 78 %; Mp: 245–247 °C; IR (KBr, cm^{-1}): 3211, 1723, 1696, 1127. ^{1}H NMR (400 MHz, DMSO-d_6) δ (ppm): 11.57 (s, 1H, NH), 8.34 (s, 1H, H (Imine)), 7.99 (s, 1H, H (triazole)), 7.69 (d, J = 9.0 Hz, 2H, $H_{2'}$, $H_{6'}$), 7.63–7.59 (d, J = 8.3 Hz, 2H, $H_{3''}$, $H_{5''}$), 7.30 (d, J = 8.3 Hz, 2H, $H_{2''}$, $H_{6''}$), 7.12 (d, J = 9.0 Hz, 2H, $H_{3'}$, $H_{5'}$), 6.88–6.79 (m, 2H, H_6, H_8), 6.17 (s, 1H, H_3), 5.63 (s, 2H, CH_2), 5.30 (s, 2H, CH_2), 5.21 (s, 2H, CH_2), 2.64 (s, 3H, CH_3 (7)), 2.37 (s, 3H, CH_3 (4)). ^{13}C NMR (100 MHz, DMSO-d_6) δ (ppm): 168.6, 160.0, 157.1, 155.0, 154.8, 144.3, 143.5, 143.2, 135.8, 132.2, 130.7, 129.7, 129.0, 127.3, 125.3, 121.9, 115.5, 113.3, 110.2, 109.5, 108.3, 66.3, 61.6, 52.5, 24.3, 21.8. Anal. calcd. for $C_{30}H_{26Br}N_5O_6$: C, 58.45; H, 4.25; N, 11.36. Found: C, 58.48; H, 4.22; N, 11.31.

(E)-N'-(3-((1-Benzyl-1H-1,2,3-triazol-4-yl)methoxy)benzylidene)-2-((4,7-dimethyl-2-oxo-2H-chromen-5-yl)oxy)acetohydrazide (13f).

White solid; Yield 85 %; Mp: 200–202 °C; IR (KBr, cm^{-1}): 3217, 3085, 1720, 1698, 1128. ^{1}H NMR (400 MHz, DMSO-d_6) δ (ppm): 11.77 (s, 1H, NH), 8.38 (s, 1H, H (Imine)), 8.06 (s, 1H, H (triazole)), 7.47–6.88 (m, 11H, $H_{2'}$, $H_{4'}$, $H_{5'}$, $H_{6'}$, $H_{2''}$, $H_{3''}$, $H_{4''}$, $H_{5''}$, $H_{6''}$, H_6, H_8), 6.22 (s, 1H, H_3), 5.70 (s, 2H, CH_2), 5.38 (s, 2H, CH_2), 5.28 (s, 2H, CH_2), 2.70 (s, 3H, CH_3 (7)), 2.38 (s, 3H, CH_3 (4)). ^{13}C NMR (100 MHz,

DMSO-d_6) δ (ppm): 168.5, 159.5, 158.2, 156.5, 154.5, 154.2, 143.6, 143.0, 142.8, 136.0, 135.3, 129.9, 128.7, 128.1, 127.8, 124.7, 120.1, 116.7, 113.0, 112.8, 112.1, 109.6, 109.0, 108.7, 107.8, 65.9, 61.0, 52.7, 23.8, 21.3. Anal. calcd. for $C_{30}H_{27}N_5O_5$: C, 67.03; H, 5.06; N, 13.03. Found: C, 67.13; H, 5.11; N, 12.93. MS: *m/z* (%); 537.4 (M^+, 0.2), 409.3 (11.3), 302.1 (32.3), 190.1 (20.5), 145.1 (29.4), 113.1 (100).

(E)-N'-(3-((1-(4-Chlorobenzyl)-1H-1,2,3-triazol-4-yl)methoxy)benzylidene)-2-((4,7-dimethyl-2-oxo-2H-chromen-5-yl)oxy)acetohydrazide (13g).

White solid; Yield 80 %; Mp: 208–210 °C; IR (KBr, cm^{-1}): 3299, 1728, 1686, 1129. ^{1}H NMR (400 MHz, DMSO-d_6) δ (ppm): 11.78 (s, 1H, NH), 8.40 (s, 1H, H (Imine)), 8.08 (s, 1H, H (triazole)), 7.53–6.9 (m, 10H, $H_{2'}$, $H_{4'}$, $H_{5'}$, $H_{6'}$, $H_{2''}$, $H_{3''}$,$H_{5''}$, $H_{6''}$, H_6, H_8), 6.24 (s, 1H, H_3), 5.72 (s, 2H, CH_2), 5.40 (s, 2H, CH_2), 5.29 (s, 2H, CH_2), 2.72 (s, 3H, CH_3 (7)), 2.40 (s, 3H, CH_3 (4)). ^{13}C NMR (100 MHz, DMSO-d_6) δ (ppm): 168.5, 159.5, 158.2, 156.5, 154.5, 154.2, 143.6, 143.0, 135.3, 134.9, 132.8, 129.8, 128.7, 124.7, 120.1, 116.7, 112.9, 112.8, 112.1, 109.9, 109.6, 108.9, 107.8, 67.0, 61.0, 51.9, 23.8, 21.3. Anal. calcd. for $C_{30}H_{26}ClN_5O_5$: C, 62.99; H, 4.58; N, 12.24. Found: C, 63.05; H, 4.61; N, 12.33.

(E)-2-((4,7-Dimethyl-2-oxo-2H-chromen-5-yl)oxy)-N'-(3-((1-(4-methylbenzyl)-1H-1,2,3-triazol-4-yl)methoxy)benzylidene)acetohydrazide (13h).

White solid; Yield 85 %; Mp: 200–202 °C; IR (KBr, cm^{-1}): 3311, 2926, 1722, 1687, 1130. ^{1}H NMR (400 MHz, DMSO-d_6) δ (ppm): 11.75 (s, 1H, NH), 8.32 (s, 1H, H (Imine)), 8.04 (s, 1H, H (triazole)), 7.48 (s, 1H, $H_{2'}$), 7.40–6.76 (m, 9H, $H_{4'}$, $H_{5'}$, $H_{6'}$, $H_{2''}$, $H_{3''}$,$H_{5''}$, $H_{6''}$, H_6, H_8), 6.20 (s, 1H, H_3), 5.61 (s, 2H, CH_2), 5.35 (s, 2H, CH_2), 5.25 (s, 2H, CH_2), 2.68 (s, 3H, CH_3 (7)), 2.36 (s, 3H, CH_3 (4)), 2.33 (s, CH_3 (4")). ^{13}C NMR (100 MHz, DMSO-d_6) δ (ppm): 168.5, 159.6, 158.2, 156.5, 154.5, 154.2, 143.5, 143.0, 142.8, 137.4, 135.3, 132.9, 129.9, 129.2, 127.9, 124.5, 120.1, 116.7, 112.8, 112.1, 109.6, 109.0, 107.8, 65.9, 61.0, 52.6, 23.8, 21.3, 20.6. Anal. calcd. for $C_{31}H_{29}N_5O_5$: C, 67.50; H, 5.30; N, 12.70. Found: C, 67.43; H, 5.36; N, 12.83. MS: *m/z* (%); 551.5 (M^+, 0.3), 302.1 (16.3), 362.2 (14.1), 190.1 (100), 145.1 (46.4), 113.1 (60.8).

(E)-2-((4,7-Dimethyl-2-oxo-2H-chromen-5-yl)oxy)-N'-(3-((1-(4-fluorobenzyl)-1H-1,2,3-triazol-4-yl)methoxy)benzylidene)acetohydrazide (13i).

White solid; Yield 75 %; Mp: 235–237 °C; IR (KBr, cm^{-1}): 3299, 1728, 1686, 1134. ^{1}H NMR (400 MHz, DMSO-d_6) δ (ppm): 11.71 (s, H, NH), 8.32 (s, 1H, H (Imine)), 8.00 (s, 1H, H (triazole)), 7.45–6.71 (m, 10H, $H_{2'}$, $H_{4'}$, $H_{5'}$, $H_{6'}$, $H_{2''}$, $H_{3''}$,$H_{5''}$, $H_{6''}$, H_6, H_8), 6.20 (s, 1H, H_3), 5.63 (s, 2H), 5.33 (s, 2H, CH_2), 5.22 (s, 2H, CH_2), 2.60 (s, 3H, CH_3 (7)), 2.37 (s, 3H, CH_3 (4)). ^{13}C NMR (100 MHz, DMSO-d_6) δ (ppm): 168.5, 159.6, 159.5, 158.2, 156.5, 156.3, 154.5, 154.2, 143.6, 143.0, 143.0, 142.9, 135.3, 130.2, 130.1, 129.9, 124.6, 120.1, 115.7, 115.5, 112.9, 112.1, 110.0, 108.9, 107.9, 67.0, 61.0, 51.9, 23.7, 21.3. Anal. calcd. for $C_{30}H_{26}FN_5O_5$: C, 64.86; H, 4.72; N, 12.61. Found: C, 64.73; H, 4.66; N, 12.63.

(E)-N'-(3-((1-(4-Bromobenzyl)-1H-1,2,3-triazol-4-yl)methoxy)benzylidene)-2-((4,7-dimethyl-2-oxo-2H-chromen-5-yl)oxy)acetohydrazide (13j).

White solid; Yield 80 %; Mp: 206–208 °C; IR (KBr, cm^{-1}): 3226, 2928, 1721, 1692, 1130. ^{1}H NMR (400 MHz, DMSO-d_6) δ (ppm): 11.77 (s, 1H, NH), 8.39 (s, 1H, H (Imine)), 8.07 (s, 1H, H (triazole)), 7.65 (d, $J = 8.2$ Hz, 2H, $H_{3''}$, $H_{5''}$), 7.50 (s, 1H, $H_{2'}$), 7.45–7.17 (m, 5H, $H_{2''}$, $H_{6''}$, $H_{4'}$, $H_{5'}$, $H_{6'}$), 6.93–6.86 (m, 2H, H_6, H_8), 6.23 (s, 1H, H_3), 5.69 (s, 2H, CH_2), 5.39 (s, 2H, CH_2), 5.28 (s, 2H, CH_2), 2.70 (s, 3H, CH_3 (7)), 2.38 (s, 3H, CH_3 (4)). ^{13}C NMR (100 MHz, DMSO-d_6) δ (ppm): 168.5, 159.5, 158.2, 156.5, 154.5, 154.2, 143.6, 143.0, 135.4, 135.3, 131.6, 130.2, 130.1, 129.9, 124.7, 121.4, 120.1, 116.6, 112.8, 112.1, 109.6, 109.0, 107.8, 65.9, 61.0, 52.0, 23.8, 21.3. for $C_{31}H_{28}BrN_5O_5$: C, 58.45; H, 4.25; N, 11.36. Found: C, 58.48; H, 4.29; N, 11.26.

(E)-N'-(4-((1-Benzyl-1H-1,2,3-triazol-4-yl)methoxy)-3-methoxybenzylidene)-2-((4,7-dimethyl-2-oxo-2H-chromen-5-yl)oxy)acetohydrazide (13k).

White solid; Yield 85 %; Mp: 249–251 °C; IR (KBr, cm^{-1}): 3220, 1727, 1694, 1491, 1125. ^{1}H NMR (400 MHz, DMSO-d_6) δ (ppm): 11.61 (s, 1H, NH), 8.32 (s, 1H, H (Imine)), 7.96 (s, 1H, H (triazole)), 7.38–7.22 (m, 8H, $H_{2'}$, $H_{5'}$, $H_{6'}$, Benzyl), 6.88–6.78 (m, 2H, H_6, H_8), 6.16 (s, 1H, H_3), 5.64 (s, 2H, CH_2), 5.32 (s, 2H, CH_2), 5.18 (s, 2H, CH_2), 3.78 (s, 3H, OCH_3), 2.63 (s, 3H, CH_3 (7)), 2.36 (s, 3H, CH_3 (4)). ^{13}C NMR (100 MHz, DMSO-d_6) δ (ppm): 168.7, 160.0, 157.1, 155.0, 154.7, 149.9, 149.6, 144.4, 143.6, 143.5, 143.1, 136.4, 129.2, 128.6, 128.4, 127.6, 125.4, 121.5, 113.5, 113.3, 110.6, 110.1, 108.3, 66.4, 62.0, 55.8, 53.3, 24.3, 21.8. Anal. calcd. for $C_{31}H_{29}N_5O_6$: C, 65.60; H, 5.15; N, 12.34. Found: C, 65.53; H, 5.22; N, 12.26. MS: *m/z* (%); 567.4 (M^+, 0.5), 409.2 (5.8), 247.0 (5.5), 190.1 (25.5), 144.2 (35.8), 91.1 (100).

(E)-N'-(4-((1-(4-Chlorobenzyl)-1H-1,2,3-triazol-4-yl)methoxy)-3-methoxybenzylidene)-2-((4,7-dimethyl-2-oxo-2H-chromen-5-yl)oxy)acetohydrazide (13l).

White solid; Yield 90 %; Mp: 280–282 °C; IR (KBr, cm^{-1}): 3318, 2921, 1729, 1694, 1130. ^{1}H NMR (400 MHz, DMSO-d_6) δ (ppm): 11.61 (s, 1H, NH), 8.33 (s, 1H, H (Imine)), 7.97 (s, 1H, H (triazole)), 7.48–7.22 (m, 7H, $H_{2'}$, $H_{5'}$, $H_{6'}$, $H_{2''}$, $H_{3''}$, $H_{5''}$, $H_{6''}$), 6.88–6.79 (m, 2H, H_6, H_8), 6.18 (s, 1H, H_3), 5.64 (s, 2H, CH_2), 5.33 (s, 2H, CH_2), 5.19 (s, 2H, CH_2), 3.79 (s, 3H, OCH_3), 2.64 (s, 3H, CH_3 (7)), 2.37 (s, 3H, CH_3 (4)). Anal. calcd. for $C_{31}H_{28}ClN_5O_6$: C, 61.85; H, 4.69; N, 11.63. Found: C, 61.88; H, 4.62; N, 11.55.

(E)-2-((4,7-Dimethyl-2-oxo-2H-chromen-5-yl)oxy)-N'-(3-methoxy-4-((1-(4-methylbenzyl)-1H-1,2,3-triazol-4-yl)methoxy)benzylidene)acetohydrazide (13m).

White solid; Yield 88 %; Mp: 250–252 °C; IR (KBr, cm^{-1}): 3320, 2923, 1728, 1692, 1130. ^{1}H NMR (400 MHz, DMSO-d_6) δ (ppm): 11.60 (s, 1H, NH), 8.28 (s, 1H, H (Imine)), 7.96 (s, 1H, H (triazole)), 7.34–7.19 (m, 7H, $H_{2'}$, $H_{5'}$, $H_{6'}$, $H_{2''}$, $H_{3''}$, $H_{5''}$, $H_{6''}$), 6.88–6.79 (m, 2H, H_6, H_8), 6.18 (s, 1H, H_3), 5.58 (s, 2H, CH_2), 5.31 (s, 2H, CH_2), 5.17 (s, 2H, CH_2), 3.78 (s, 3H, OCH_3), 2.64 (s, 3H, CH_3 (7)), 2.37 (s, 3H, CH_3 (4)), 2.30 (s, 3H, CH_3 (4″)). ^{13}C NMR (100 MHz, DMSO-d_6) δ (ppm): 160.1, 157.1, 155.1, 143.5, 138.0, 133.4, 129.7, 128.5, 127.7, 125.2, 113.3, 110.6, 110.2, 108.8, 62.0, 55.8, 53.1, 43.6, 24.3, 21.8, 21.1. Anal. calcd. for $C_{32}H_{31}N_5O_6$: C, 66.08; H, 5.37; N, 12.03. Found: C, 66.18; H, 5.32; N, 12.11. MS: *m/z* (%); 581.4 (M^+, 0.25), 534.2 (6.3), 288.0 (5.9), 191.1 (100).

(E)-2-((4,7-Dimethyl-2-oxo-2H-chromen-5-yl)oxy)-N'-(4-((1-(4-fluorobenzyl)-1H-1,2,3-triazol-4-yl)methoxy)-3-

methoxybenzylidene)acetohydrazide (13n).

White solid; Yield 82 %; Mp: 272–274 °C; IR (KBr, cm^{-1}): 3325, 2934, 1729, 1694, 1130. ^{1}H NMR (400 MHz, DMSO-d_6) δ (ppm): 11.61 (s, 1H, NH), 8.32 (s, 1H, H (Imine)), 7.96 (s, 1H, H (triazole)), 7.45–7.22 (m, 7H, $H_{2'}$, $H_{5'}$, $H_{6'}$, $H_{2''}$, $H_{3''}$, $H_{5''}$, $H_{6''}$), 6.88–6.78 (m, 2H, H_6, H_8), 6.17 (s, 1H, H_3), 5.63 (s, 2H, CH_2), 5.32 (s, 2H, CH_2), 5.18 (s, 2H, CH_2), 3.78 (s, 3H, OCH_3), 2.64 (s, 3H, CH_3 (7)), 2.36 (s, 3H, CH_3 (4)). ^{13}C NMR (100 MHz, DMSO-d_6) δ (ppm): 168.8, 155.1, 150.3, 149.7, 147.9, 143.5, 143.2, 130.6, 125.3, 121.7, 116.1, 115.9, 113.4, 112.9, 109.3, 109.0, 61.9, 55.5, 52.6, 24.0, 21.7. Anal. calcd. for $C_{31}H_{28}FN_5O_5$: C, 63.58; H, 4.82; N, 11.96. Found: C, 63.45; H, 4.77; N, 12.06. MS: *m/z* (%); 585.3 (M^+, 0.2), 396.2 (8.1), 247.0 (4.1), 190.1 (28.5), 162.1 (50.8), 109.1 (100).

(E)-N'-(4-((1-(4-Bromobenzyl)-1H-1,2,3-triazol-4-yl)methoxy)-3-methoxybenzylidene)-2-((4,7-dimethyl-2-oxo-2H-chromen-5-yl)oxy)acetohydrazide (13o).

White solid; Yield 82 %; Mp: 218–220 °C; IR (KBr, cm^{-1}): 3322, 2922, 1729, 1693, 1130. ^{1}H NMR (400 MHz, DMSO-d_6) δ (ppm): 11.61 (s, 1H, NH), 8.32 (s, 1H, H (Imine)), 7.96 (s, 1H, H (triazole)), 7.64–7.59 ((d, J = 8.4 Hz, 2H, $H_{3''}$, $H_{5''}$), 7.35–7.22 (m, 5H, $H_{2''}$, $H_{6''}$, $H_{2'}$, $H_{5'}$, $H_{6'}$), 6.89–6.79 (m, 2H, H_6, H_8), 6.17 (s, 1H, H_3), 5.63 (s, 2H, CH_2), 5.32 (s, 2H, CH_2), 5.18 (s, 2H, CH_2), 3.79 (s, 3H, OCH_3), 2.64 (s, 3H, CH_3 (7)), 2.37 (s, 3H, CH_3 (4)). ^{13}C NMR (100 MHz, DMSO-d_6) δ (ppm): 168.8, 159.8, 157.2, 155.0, 150.1, 149.7, 143.5, 138.8, 138.3, 135.8, 135.6, 132.1, 130.7, 125.4, 121.9, 113.9, 111.6, 109.5, 62.0, 55.8, 52.5, 49.7, 24.3, 21.8. Anal. calcd. for $C_{30}H_{26}BrN_5O_5$: C, 57.59; H, 4.37; N, 10.83. Found: C, 57.83; H, 4.43; N, 10.79.

4.2. In vitro urease inhibition assay

The jack bean urease (EC 3.5.1.5) enzyme was purchased from Sigma–Aldrich (USA). The absorbance spectra were recorded on a Synergy H1 Hybrid multi-mode microplate reader. Urease inhibitory activity of the synthesized compounds were measured at the concentration of 1, 10, and 100 μM, using the modified Berthelot spectrophotometric method at 625 nm [44]. Thiourea was used as the reference standard inhibitor. In this method ammonia (NH_3) react with hypochlorite (OCl^-) to produce monochloramine, which then reacts with phenol to produce blue-colored indophenols. The all-synthesized compounds and thiourea were dissolved in deionized water with a maximum of 5 % DMSO. The assay mixture consisted of 850 μl of urea (30 mM) in a 100 mM phosphate buffer (pH 7.4) and 100 μl of test compounds in the same buffer, resulting in a total volume of 950 μl. After incubating for 30 min at 37 °C, the reactions were initiated by adding 15 μl of urease enzyme solution (3 mg/ml in 100 mM phosphate buffer, pH 7.4). Urease activity was assessed by measuring the ammonia concentration after 30 min of enzymatic reaction. The ammonia concentration was measured by adding 100 μl of the incubated solution to a mixture of 500 μl of solution A (which contained 5.0 g of phenol and 25 mg of sodium nitroprusside in 500 ml of distilled water) and 500 μl of solution B (which included 2.5 g of sodium hydroxide and 4.2 ml of sodium hypochlorite [5 % chlorine] in 500 ml of distilled water). This mixture was then incubated at 37 °C for an additional 30 min. The absorbance of developed blue- colored indophenols was read at 625 nm. The activity of uninhibited urease was established as the control, representing 100 % activity. The percentage of inhibition was calculated using formula [1−(T/C)] × 100, where T and C represent the absorbance of the test compound and the solvent (used as a negative control) in the presence of the enzyme, respectively. All data were obtained from three independent experiments and analyzed using SPSS and GraphPad Prism 5 software.

4.3. In vitro kinetic assay

To assess the type of urease inhibition exhibited by the most potent compound, we employed Lineweaver–Burk plots as outlined in the literature. Urease inhibition was evaluated by varying urea concentrations (3.2 – 100 mM) in the presence of different concentrations of the most effective compound (0, 1, 2, and 4 μM). The inhibitory constant (Ki) was calculated through secondary replotting of the Lineweaver–Burk plots. All data were obtained in triplicate to ensure reliability [44].

4.4. Docking study

The rigid-ligand docking studies were conducted using AutoDock 4.2 and AutoDock Tools 1.5.4 (ADT) (Morris et al., 2009; Sanner, 1999). The 3D structure of 13a was optimized using the DFT method with the BP86/DEF2-TZVP basis set in the ORCA quantum chemistry package (Neese, 2012). The 3D structure of 13a was then converted to PDBQT format using AutoDockTools (ADT), which added essential information about atom types and charges. The target protein structure (PDB ID: 3la4, resolution: 2.05 Å) was obtained from the RCSB PDB database. Water molecules and other non-essential heteroatoms were removed, polar hydrogens were added, and Kollman partial atomic charges were assigned to the protein. The protein structure was subsequently converted to PDBQT format. A grid box was defined to encompass the active site of the protein using AutoGrid, with dimensions set at 60 × 60 × 60 and center coordinates at x: 38.205, y: 45.194, and z: 75.174 to adequately cover the binding site residues. The Lamarckian Genetic Algorithm (LGA) was selected to model the interactions between the receptor and the ligand, with the following settings: Population size: 150, Number of evaluations: 25,000,000, Number of generations: 27,000, Mutation rate: 0.02, Crossover rate: 0.8, Number of docking runs: 100.

4.5. MD simulations

Molecular dynamics (MD) simulations were conducted using GROMACS 2019 to investigate the stability and behavior of the protein-ligand complex. The ligand was parameterized using the CGenFF server, compatible with the CHARMM36 force field. The protein-ligand complex was placed in a dodecahedron box, solvated with the TIP3P water model, and neutralized with 11 Na^+ counter

ions. Energy minimization was performed using the steepest descent algorithm, followed by a two-phase equilibration process. First, an NVT ensemble (constant Number of particles, Volume, and Temperature) for 100 ps at 300 K using the V-rescale thermostat, followed by an NPT ensemble (constant Number of particles, Pressure, and Temperature) for 300 ps at 1 bar using the Parrinello-Rahman barostat (Parrinello & Rahman, 1981). Temperature was controlled using the modified V-rescale thermostat from Berendsen (Berendsen et al., 1984). Position restraints were applied to the protein heavy atoms during equilibration. The production MD simulation was run for 100 ns at 300 K and 1 atm, with an additional 20 ns simulation of apoenzyme to analyze the stability of Ni ions in the binding site, and the compatibility of the force field and simulation conditions with the urease enzyme. The LINCS algorithm was used to constrain bond lengths, and the Particle Mesh Ewald method was used for long-range electrostatic interactions. The root mean square deviation (RMSD) of the protein backbone and ligand, as well as the root mean square fluctuation (RMSF) of protein residues, were calculated to assess structural stability and flexibility.

4.6. Prediction of ADME and drug likeness studies

In silico ADME parameters of the synthesized compounds were studied using by SwissADME online server (http://www. swissadme. ch) and pkCSM online server (https://biosig.lab.uq.edu.au/pkcsm/)

CRediT authorship contribution statement

Hassan Sepehrmansourie: Investigation, Formal analysis, Data curation, Conceptualization, Methodology, Writing – original draft. **Mohammad Azimi:** Software, Conceptualization, Resources, Writing – original draft. **Ahmad Ebadi:** Supervision, Software, Conceptualization, Resources. **Gholamabbas Chehardoli:** Investigation. **Mohammad Ali Zolfigol:** Methodology, Visualization. **Massoud Amanlou:** Formal analysis, Data curation, Validation, Visualization. **Mohammad Nazari Montazer:** Data curation, Formal analysis, Validation, Visualization. **Mohammad Mahdavi:** Methodology, Visualization. **Zahra Najafi:** Writing – review & editing, Visualization, Supervision, Project administration, Conceptualization, Investigation.

Data availability statement

All data included in article/supplementary material in article:

Funding statement

This work was supported by Vice-chancellor for Research and Technology of Hamadan University of Medical Sciences, Hamadan, Iran with project No. 1402121511061.

Declaration of competing interest

The authors declare the following financial interests/personal relationships which may be considered as potential competing interests:Zahra Najafi reports financial support was provided by Hamadan University of Medical Sciences. If there are other authors, they declare that they have no known competing financial interests or personal relationships that could have appeared to influence the work reported in this paper.

Acknowledgments

The authors express their gratitude to the Vice-Chancellor for Research and Technology at Hamadan University of Medical Sciences, Hamadan, Iran, for funding this work through grant no. 1402121511061.

Appendix A. Supplementary data

Supplementary data to this article can be found online at https://doi.org/10.1016/j.heliyon.2024.e41321.

References

[1] S. Ahmad, M. Khan, N.U. Rehman, M. Ikram, S. Rehman, M. Ali, J. Uddin, A. Khan, A. Alam, A.J.M. Al-Harrasi, Design, synthesis, crystal structure, in vitro and in silico evaluation of new N′-benzylidene-4-tert-butylbenzohydrazide derivatives as potent urease inhibitors, Molecules 27 (20) (2022) 6906, https://doi.org/10.3390/molecules27206906.

[2] R. Ahmad, M. Khan, A. Alam, A.A. Elhenawy, A. Qadeer, A.F. AlAsmari, M. Alharbi, F. Alasmari, M.J.S.P.J. Ahmad, Synthesis, molecular structure and urease inhibitory activity of novel bis-Schiff bases of benzyl phenyl ketone: a combined theoretical and experimental approach, Saudi Pharmaceut. J. 31 (8) (2023) 101688, https://doi.org/10.1016/j.jsps.2023.06.021.

[3] A. Khan, A.A. Elhenawy, M.U. Rehman, M. Alam, A. Alam, N.U. Rehman, M. Ibrahim, Synthesis of novel 2-mercapto-1,3,4-oxadiazole derivatives as potent urease inhibitors: in vitro and in silico investigations, J. Mol. Struct. 1312 (2024) 138596, https://doi.org/10.1016/j.molstruc.2024.138596.

[4] S. Ahmad, M. Khan, A. Alam, A. Ajmal, A. Wadood, A. Khan, A.F. AlAsmari, M. Alharbi, A. Alshammari, A.J.R.a. Shakoor, Novel flurbiprofen clubbed oxadiazole derivatives as potential urease inhibitors and their molecular docking study, RSC Adv. 13 (37) (2023) 25717–25728, https://doi.org/10.1039/D3RA03841F.

[5] S. Hu, S. Jiang, X. Qi, R. Bai, X.Y. Ye, T.J.D.D.R. Xie, Races of small molecule clinical trials for the treatment of COVID-19: an up-to-date comprehensive review, Drug Dev. Res. 83 (1) (2022) 16–54, https://doi.org/10.1002/ddr.21895.

[6] S. Ahmad, M. Khan, M.I.A. Shah, M. Ali, A. Alam, M. Riaz, K.M.J.A.o. Khan, Synthetic transformation of 2-{2-fluoro [1, 1′-biphenyl]-4-yl} propanoic acid into hydrazide–hydrazone derivatives: in vitro urease inhibition and in silico study, ACS Omega 7 (49) (2022) 45077–45087, https://doi.org/10.1021/acsomega.2c05498.

[7] L. Chen, Z. Jiang, L. Yang, Y. Fang, S. Lu, O.U. Akakuru, S. Huang, J. Li, S. Ma, A.J. Wu, HPDA/Zn as a CREB inhibitor for ultrasound imaging and stabilization of atherosclerosis plaque, Chin. J. Chem. 41 (2) (2023) 199–206, https://doi.org/10.1002/cjoc.202200406.

[8] P. Kafarski, M. Talma, Recent advances in design of new urease inhibitors: a review, J. Advan. Res., J. Adv. Res. 13 (2018) 101–112, https://doi.org/10.1016/j.jare.2018.01.007.

[9] C. Montecucco, R. Rappuoli, Living dangerously: how Helicobacter pylori survives in the human stomach, Nat. Rev. Mol. Cell Biol. 2 (6) (2001) 457–466, https://doi.org/10.1038/35073084.

[10] H.L. Mobley, G.L. Mendz, S.L. Hazell, Helicobacter pylori: physiology and genetics, 2001.

[11] M. Islam, A. Khan, M.T. Shehzad, M. Khiat, S.A. Halim, A. Hameed, S.R. Shah, R. Basri, M.U. Anwar, J. Hussain, Therapeutic potential of N4-substituted thiosemicarbazones as new urease inhibitors: biochemical and in silico approach, Bioorg. Chem. 109 (2021) 104691, https://doi.org/10.1016/j.bioorg.2021.104691.

[12] A. Mirzaei, B. Nasr Esfahani, A. Raz, M. Ghanadian, S. Moghim, From the urinary catheter to the prevalence of three classes of integrons, β-lactamase genes, and differences in antimicrobial susceptibility of Proteus mirabilis and clonal relatedness with Rep-PCR, BioMed Res. Int. 2021 (1) (2021) 9952769, https://doi.org/10.1155/2021/9952769.

[13] S. Ahmad, M. Khan, M.I.A. Shah, M. Ali, A. Alam, M. Riaz, K.M. Khan, Synthetic transformation of 2-{2-Fluoro[1,1′-biphenyl]-4-yl} propanoic acid into hydrazide–hydrazone derivatives: in vitro urease inhibition and in silico study, ACS Omega 7 (49) (2022) 45077–45087, https://doi.org/10.1021/acsomega.2c05498.

[14] A. Balasubramanian, K.J. Ponnuraj, Crystal structure of the first plant urease from jack bean: 83 years of journey from its first crystal to molecular structure, J. Mol. Biol. 400 (3) (2010) 274–283, https://doi.org/10.1016/j.jmb.2010.05.009.

[15] M. Ayaz, A. Alam, Zainab, A.A. Elhenawy, N. Ur Rehman, S. Ur Rahman, M. Ali, A. Latif, A. Al-Harrasi, M.J.C. Ahmad, Biodiversity, designing and synthesis of novel fexofenadine-derived hydrazone-schiff bases as potential urease inhibitors: in-vitro, molecular docking and DFT investigations, Chem. Biodiversity 21 (8) (2024) e202400704, https://doi.org/10.1002/cbdv.202400704.

[16] S. Ahmad, M. Abdul Qadir, M. Ahmed, M. Imran, M. Ahmad, N. Yousaf, T.A. Wani, S. Zargar, I. Ali, M. Muddassar, Exploring the potential of new benzamide-acetamide pharmacophore containing sulfonamide as urease inhibitors: structure–activity relationship, kinetics mechanism, and in silico studies, ACS Omega 8 (48) (2023) 46165–46181, https://doi.org/10.1021/acsomega.3c07275.

[17] S. Ahmad, M. Abdul Qadir, M. Ahmed, M. Imran, N. Yousaf, T.A. Wani, S. Zargar, I. Ali, M. Muddassar, Exploring the potential of propanamide-sulfonamide based drug conjugates as dual inhibitors of urease and cyclooxygenase-2: biological and their in silico studies, Front. Chem. 11 (2023), https://doi.org/10.3389/fchem.2023.1206380.

[18] S. Ahmad, M. Abdul Qadir, M. Ahmed, M. Imran, N. Yousaf, T.A. Wani, S. Zargar, I. Ali, M. Muddassar, New acetamide-sulfonamide-containing scaffolds: antiurease activity screening, structure-activity relationship, kinetics mechanism, molecular docking, and MD simulation studies, Molecules 28 (14) (2023) 5389, https://doi.org/10.3390/molecules28145389.

[19] S. Ahmad, M. Khan, N.U. Rehman, M. Ikram, S. Rehman, M. Ali, J. Uddin, A. Khan, A. Alam, A. Al-Harrasi, Design, synthesis, crystal structure, in vitro and in silico evaluation of new N′-Benzylidene-4-tert-butylbenzohydrazide derivatives as potent urease inhibitors, Molecules 27 (20) (2022) 6906, https://doi.org/10.3390/molecules27206906.

[20] R.H. Vekariya, H.D. Patel, Recent advances in the synthesis of coumarin derivatives via Knoevenagel condensation: a review, Synth. Commun. 44 (19) (2014) 2756–2788, https://doi.org/10.1080/00397911.2014.926374.

[21] A. Stefanachi, F. Leonetti, L. Pisani, M. Catto, A. Carotti, Coumarin: a natural, privileged and versatile scaffold for bioactive compounds, Molecules 23 (2) (2018) 250, https://doi.org/10.3390/molecules23020250.

[22] U. Salar, B. Qureshi, K.M. Khan, M.A. Lodhi, Z. Ul-Haq, F.A. Khan, F. Naz, M. Taha, S. Perveen, Sh Hussain, Aryl hydrazones linked thiazolyl coumarin hybrids as potential urease inhibitors, J. Iran. Chem. Soc. 19 (4) (2022) 1221–1238, https://doi.org/10.1007/s13738-021-02377-8.

[23] W. Yang, Q. Feng, Z. Peng, G.J. Wang, An overview on the synthetic urease inhibitors with structure-activity relationship and molecular docking, Eur. J. Med. Chem. 234 (2022) 114273, https://doi.org/10.1016/j.ejmech.2022.114273.

[24] F. Naz, M. Latif, U. Salar, K.M. Khan, M. Al-Rashida, I. Ali, B. Ali, M. Taha, S.J.B.C. Perveen, 4-Oxycoumarinyl linked acetohydrazide Schiff bases as potent urease inhibitors, Bioorg. Chem. 105 (2020) 104365, https://doi.org/10.1016/j.bioorg.2020.104365.

[25] G. Aromí, L.A. Barrios, O. Roubeau, P.J.C.C.R. Gamez, Triazoles and tetrazoles: prime ligands to generate remarkable coordination materials, Coord. Chem. Rev. 255 (5–6) (2011) 485–546, https://doi.org/10.1016/j.ccr.2010.10.038.

[26] P.L. Golas, K.J.C.S.R. Matyjaszewski, Marrying click chemistry with polymerization: expanding the scope of polymeric materials, Chem. Soc. Rev. 39 (4) (2010) 1338–1354, https://doi.org/10.1039/B901978M.

[27] A.H. El-Sagheer, T.J.C.S.R. Brown, Click chemistry with DNA, Chem. Soc. Rev. 39 (4) (2010) 1388–1405, https://doi.org/10.1039/B901971P.

[28] M. Finn, V.V. Fokin, Click chemistry: function follows form, Chem. Soc. Rev. 39 (4) (2010) 1231–1232, https://doi.org/10.1039/C003740K.

[29] H.C. Kolb, K.B. Sharpless, The growing impact of click chemistry on drug discovery, Drug Discov. Today 8 (24) (2003) 1128–1137, https://doi.org/10.1016/S1359-6446(03)02933-7.

[30] S. Moghimi, F. Goli-Garmroodi, M. Allahyari-Devin, H. Pilali, M. Hassanzadeh, S. Mahernia, M. Mahdavi, L. Firoozpour, M. Amanlou, A. Foroumadi, Synthesis, evaluation, and molecular docking studies of aryl urea-triazole-based derivatives as anti-urease agents, Arch. Pharm. 351 (7) (2018) 1800005, https://doi.org/10.1002/ardp.201800005.

[31] M.S. Asgari, H. Azizian, M. Nazari Montazer, M. Mohammadi-Khanaposhtani, M. Asadi, S. Sepehri, P.R. Ranjbar, R. Rahimi, M. Biglar, B.J.A.d.P. Larijani, New 1, 2, 3-triazole–(thio) barbituric acid hybrids as urease inhibitors: design, synthesis, in vitro urease inhibition, docking study, and molecular dynamic simulation, Arch. Pharm. 353 (9) (2020) 2000023, https://doi.org/10.1002/ardp.202000023.

[32] E.B. Rezaei, F. Abedinifar, H. Azizian, M.N. Montazer, M. Asadi, S. Hosseini, S. Sepehri, M. Mohammadi-Khanaposhtani, M. Biglar, B.J.C.P. Larijani, Design, synthesis, and evaluation of metronidazole-1, 2, 3-triazole derivatives as potent urease inhibitors, Chem. Pap. 75 (2021) 4217–4226, https://doi.org/10.1007/s11696-021-01653-4.

[33] R. Ahmad, M. Khan, A. Alam, A.A. Elhenawy, A. Qadeer, A.F. AlAsmari, M. Alharbi, F. Alasmari, M. Ahmad, Synthesis, molecular structure and urease inhibitory activity of novel bis-Schiff bases of benzyl phenyl ketone: a combined theoretical and experimental approach, Saudi Pharmaceut. J. 31 (8) (2023) 101688, https://doi.org/10.1016/j.jsps.2023.06.021.

[34] R. Adams, S. Loewe, C. Jelinek, H. Wolff, Tetrahydrocannabinol homologs with marihuana activity. IX1, J. Am. Chem. Soc. 63 (7) (1941) 1971–1973, https://doi.org/10.1021/ja01852a052.

[35] A.S. Fonseca, M.S.T. Gonçalves, S.P. Costa, Phenacyl ester derivatives bearing heterocycles as models for photocleavable linkers: synthesis and photolysis studies, Tetrahedron 68 (38) (2012) 8024–8032, https://doi.org/10.1016/j.tet.2012.06.100.

[36] N. Duangdee, W. Mahavorasirikul, S. Prateeptongkum, Design synthesis and anti-proliferative activity of some new coumarin substituted hydrazide–hydrazone derivatives, J. Chem. Sci. 132 (2020) 1–12, https://doi.org/10.1007/s12039-020-01767-4.

[37] Z. Najafi, A. Ebadi, G. Chehardoli, M. Ziaei, M. khoshneviszadeh, T. Akbarzadeh, M. Saeedi, P. Gholamhoseini, M. Mahdavi, Design, synthesis, in vitro, and in silico studies of novel benzylidene 6-methoxy-1-tetralone linked to benzyloxy and benzyl -1,2,3- triazole rings as potential tyrosinase inhibitors, J. Mol. Struct. 1271 (2023) 134018, https://doi.org/10.1016/j.molstruc.2022.134018.

[38] K. Somakala, M. Amir, V. Sharma, S. Wakode, Synthesis and pharmacological evaluation of pyrazole derivatives containing sulfonamide moiety, Monatsh. fur Chem. 147 (2016) 2017–2029, https://doi.org/10.1007/s00706-016-1694-x.
[39] A. Balasubramanian, K. Ponnuraj, Crystal structure of the first plant urease from jack bean: 83 Years of journey from its first crystal to molecular structure, J. Mol. Biol. 400 (3) (2010) 274–283, https://doi.org/10.1016/j.jmb.2010.05.009.
[40] B.P. Roberts, B.R. Miller 3rd, A.E. Roitberg, K.M. Merz Jr., Wide-open flaps are key to urease activity, J. Am. Chem. Soc. 134 (24) (2012) 9934–9937, https://doi.org/10.1021/ja3043239.
[41] L. Macomber, M.S. Minkara, R.P. Hausinger, K.M. Merz Jr., Reduction of urease activity by interaction with the flap covering the active site, J. Chem. Inf. Model. 55 (2) (2015) 354–361, https://doi.org/10.1021/ci500562t.
[42] D.E. Pires, T.L. Blundell, D.B. Ascher, pkCSM: predicting small-molecule pharmacokinetic and toxicity properties using graph-based signatures, J. Med. Chem. 58 (9) (2015) 4066–4072, https://doi.org/10.1021/acs.jmedchem.5b00104.
[43] A. Daina, O. Michielin, V.J.S.r. Zoete, SwissADME: a free web tool to evaluate pharmacokinetics, drug-likeness and medicinal chemistry friendliness of small molecules, Sci. Rep. 7 (1) (2017) 42717, https://doi.org/10.1038/srep42717.
[44] H. Azizian, F. Nabati, A. Sharifi, F. Siavoshi, M. Mahdavi, M. Amanlou, Large-scale virtual screening for the identification of new Helicobacter pylori urease inhibitor scaffolds, J. Mol. Model. 18 (7) (2012) 2917–2927, https://doi.org/10.1007/s00894-011-1310-2.